Princeton Plasma Physics Laboratory

PPPL- 4955

PPPL- 4955

# External Heating and Current Drive Source Requirements towards Steady-state Operation in ITER

F.M. Poli, C.E. Kessel, P.T. Bonoli, D.B. Batchelor,
R.W. Harvey and P.B. Snyder

November 2013

PPPL PRINCETON PLASMA PHYSICS LABORATORY

**Prepared for the U.S. Department of Energy under Contract DE-AC02-09CH11466.**

# Princeton Plasma Physics Laboratory
# Report Disclaimers

---

## Full Legal Disclaimer



## Trademark Disclaimer



---

# PPPL Report Availability

## Princeton Plasma Physics Laboratory:

http://www.pppl.gov/techreports.cfm

## Office of Scientific and Technical Information (OSTI):

http://www.osti.gov/bridge

---

**Related Links:**

**U.S. Department of Energy**

**Office of Scientific and Technical Information**

**Fusion Links**

# External Heating and Current Drive source requirements towards steady-state operation in ITER

**F. M. Poli, C. E. Kessel**
Princeton Plasma Physics Laboratory, Princeton, NJ, 08543, USA.

**P. T. Bonoli**
MIT Plasma Science and Fusion Center, Cambridge, MA 02139, USA

**D. B. Batchelor**
Oak Ridge National Laboratory, Oak Ridge, TN 37831-6169, USA

**R. W. Harvey**
CompX, Box 2672, Del Mar, CA 92014, USA

**P. B. Snyder**
General Atomics, PO Box 85608, San Diego, CA 92186-5608, USA

**Abstract.** Steady state scenarios envisaged for ITER aim at optimizing the bootstrap current, while maintaining sufficient confinement and stability to provide the necessary fusion yield. Non-inductive scenarios will need to operate with Internal Transport Barriers (ITBs) in order to reach adequate fusion gain at typical currents of 9 MA. However, the large pressure gradients associated with ITBs in regions of weak or negative magnetic shear can be conducive to ideal MHD instabilities, reducing the no-wall limit. The $\mathbf{E}\times\mathbf{B}$ flow shear from toroidal plasma rotation is expected to be low in ITER, with a major role in the ITB dynamics being played by magnetic geometry. Combinations of heating and current drive (H/CD) sources that sustain reversed magnetic shear profiles throughout the discharge are the focus of this work. Time-dependent transport simulations indicate that a combination of electron cyclotron (EC) and lower hybrid (LH) waves is a promising route towards steady state operation in ITER. The LH forms and sustains expanded barriers with their foot at large radii, while the EC deposition at mid-radius freezes the bootstrap current profile stabilizing the barrier and leading to confinement levels 50% higher than typical H-mode energy confinement times. Using LH spectra with parallel refractive index in the range of 1.75-1.85, the performance of these plasma scenarios is close to the ITER target of 9 MA non-inductive current and fusion gain $Q = 5$.

PACS numbers: 52.25,52.30,52.35,52.50,52.55,52.65

## 1. Introduction

One of the ITER goals is demonstration of fully non-inductive operation in stationary conditions, up to 3000 s and with fusion gain (ratio of fusion to input power) of $Q = 5$. These advanced scenario plasmas operate at a plasma current lower than the baseline configuration (the 15 MA ELMy H-mode inductive scenario), to minimize the external heating power and current drive requirements [1].

The ITER steady state scenario targets plasmas with currents of 8-9 MA in the flat-top, with significant fraction of self-generated bootstrap current. In order to compensate for the confinement degradation that occurs with decreasing plasma current and to obtain a fusion gain $Q = 5$ at a current of 9 MA, steady state operation should achieve $\beta_{\rm N} > 2.5$ with a confinement gain factor $H_{98} > 1.5$, likely obtainable only with Internal Transport Barriers (ITBs) [2].

Plasmas with ITBs exhibit radially localized regions of improved confinement with steep pressure gradients in the plasma core, which drive large bootstrap current, generate hollow current profiles and hence negative magnetic shear in the core. Extensive reviews of the physics and of the main characteristics of ITBs observed in present day experiments are provided in the papers by Connor *et al* [3], Litaudon [4], Staebler [5] and Wolf [6].

Extrapolating present day ITB experiments to ITER is challenging because of the limited database available for densities above 85% of the Greenwald limit and for ion and electron temperatures of comparable values. The dominant ion heating from neutral beam and the presence of a significant toroidal rotation in present-day experiments set conditions for ITB formation that are different from those foreseen in ITER, where the $\mathbf{E}\times\mathbf{B}$ flow shear contribution from the toroidal rotation is expected to be low and where the energy confinement times will be longer than the electron-ion thermal equilibration time scales [3].

From present experiments with dominant electron heating it is observed that (a) the presence of reverse shear in the core is necessary for formation of ITBs in the electron channel, which (b) typically form at injected powers lowers than those at which ion barriers are observed and (c) ITBs in reversed shear plasmas have their foot locked at the radius of the minimum safety factor [3].

In particular, experiments on TCV with Electron Cyclotron (EC) heating and current drive indicate that the ITB formation is correlated with the appearance of a zero-shear region and it occurs over rapid time scales, shorter than electron energy confinement times, rather than being correlated with a progressive reduction of the magnetic shear [7, 8]. Similar results have been reported on JET where reverse shear and strong electron ITBs were formed with Lower Hybrid Current Drive (LHCD) pre-heat and sustained in the flattop with Neutral Beam Injection (NBI) [9, 10, 11].
Confinement gain values higher than $H_{98} > 1.5$ have been demonstrated experimentally on JT-60U high-$\beta_P$ plasmas. For example, stable operation with $H_{98} \sim 1.6$, $\beta_{\rm N} \sim 2.5$, weak reversed magnetic shear, an internal transport barrier at $r/a \sim 3/4$, and with 70-

80% of non-inductive current drive (1/3 NB and 2/3 bootstrap) have been demonstrated on JT-60U [12]. Experiments with ITBs in JT-60U have shown that the bootstrap current fraction increases from about 0.4 in plasmas with positive to flat reverse shear and with $q_{\min}$ slightly above 1 to 0.5 in plasma with weak reverse shear and weak ITBs and can be larger than 0.7 in plasmas with moderate to strong reverse shear and strong ITBs [13].

Heating in the ramp-up phase delays the inductive current penetration and favors the formation of magnetic shear profiles reversed in the core, which - in turn - favors the formation of ITBs. By tailoring the heating and current profiles, the target is to maintain wide ITBs at large radius. This will sustain high-pressure core plasmas with large volume within the stability limits. Conversely, strong ITBs with foot at small radius and reduced width (so-called box-type) should be avoided because the large pressure gradients are conducive to ideal MHD instabilities that reduce the no-wall limit [14, 15, 9, 10].

This paper discusses how the heating mix affects the ITB sustainment and the plasma performance towards continuous operation at the ITER goals. Prior to this work, steady state simulation scenarios with various heating mixes have been addressed by other authors [16, 17, 18, 19, 20, 21].

Novel features of the simulations described herein are (a) the pedestal height is constrained by peeling-ballooning instabilities; (b) the timing and power step-up of the external sources in the ramp-up has been formulated to favor the formation of reverse shear profiles in L-mode and the triggering of ITBs and at the same time to avoid too large a growth of the safety factor on axis; (c) the thermal diffusivity profiles are calculated self-consistently using a transport model that responds to magnetic shear profiles reversed in the core and (d) all simulations attain at maintaining the plasma in the MHD stable region during the whole discharge, based on the results from a previous work [22].

Time dependent simulations are run with the Tokamak Simulator Code TSC [23], as described in Sec.2. It will be shown in Sec.4 that LHCD sustains more expanded ITBs and plasmas with higher global confinement levels. Operating with densities close to the Greenwald limit these plasmas sustain non-inductive currents between 8 and 9 MA and achieve fusion gains of $Q > 4$ (Sec.5). It will be shown that LH is necessary to trigger and sustain expanded ITBs, but that the use of EC is necessary to stabilize the ITB foot and to freeze the bootstrap current profile at mid-radius (Sec.6.1). Configurations that combine EC and LH offer an optimum combination of pressure and current density profiles that are compatible with confinement levels $H_{98} > 1.6$ and achieve $Q \simeq 5$, thus representing a promising route towards the achievement of the ITER goals, as discussed in Sec.7.

## 2. Scenario development

Full plasma discharges are simulated with the Tokamak Simulation Code (TSC) [23], a predictive, free boundary transport evolution code. The plasma equilibrium and field evolution equations are solved on a two-dimensional Cartesian grid, while the surface-averaged transport equations for the pressure and densities are solved in magnetic flux coordinates.

TSC includes a 2D representation of the central solenoid, of the poloidal field coils and of the surrounding conducting structures, as well as feedback systems for plasma position, shape and current. TSC is used to establish the scenario in terms of all parameters as a function of time, targeting the desired properties of the scenario and attempting to remain within all limits.

### *2.1. Heating and Current Drive Sources*

The external power heating and current drive sources considered in this work are 33 MW of negative ion neutral beam (NB), 20 MW of ion cyclotron (IC), 20 MW of electron cyclotron (EC) and up to 40 MW of lower hybrid (LH). The external heating starts at 15 s, shortly after divert time, and the RF power is stepped-up in the ramp-up to reach full power level at 75 s. The NB injection begins when admissible density is reached, approximately mid-way through the ramp-up phase. At 75s the sum of the external RF power (40 MW in all configurations) plus 16.5 MW of NB is above the threshold for the L-H transition, which is enforced in TSC by modifying analytically the density profile and by dropping the thermal diffusivity at the edge to form a pedestal. The width and the height of the pedestal are set by the EPED1 peeling-ballooning stability code [24]. TSC interpolates over a look-up table of pedestal height and width values calculated with EPED1 for current in the range of 7-10 MA and pedestal density in the range of $4 - 10 \times 10^{19}$ m$^{-3}$.

Figure 1 shows an example of the time evolution of power, current and plasma parameters for a configuration with 33 MW of NB power and 20 MW each of EC and LH power, which attains steady state, with 100% non-inductive current of 8.8 MA, $Q \simeq 5$, $\beta_N \simeq 2.3$ and confinement $H_{98} = 1.65$ and that will be further described in Sec.5.

The heating and current drive profiles are calculated using modules external to TSC, which are described below. This can be done either within the SWIM IPS framework [25, 26] or using TRANSP [27]. In the former case TSC communicates directly with the H/CD codes and advances self-consistently the equilibrium and pressure profiles. In the second approach TSC provides experimental-like conditions: the equilibrium and pressure profiles are input to TRANSP, which calculates the H/CD profiles for the whole discharge. These are then given back to TSC for recalculation of the scenario, iterating the process for convergence.

*Ion Cyclotron model* The ion cyclotron wave is used in the ramp-up phase to provide heating and fast wave current in the core and to assist with the L-H transition. The IC power is stepped down in the flattop to maintain seed current in the core and avoid the formation of a current hole. The ICRH uses Helium-3 ion minority heating at a concentration of 2% of the electron density and a frequency of 48 MHz for on-axis deposition and to accommodate the strong magnetic axis shift. The ICRF source model is the TORIC full wave [28] with a Fokker Planck treatment of the resonant species (the FPPRF code [29]) and equivalent Maxwellian for other fast species (neutral beam ions and alpha particles).

*Neutral Beam model* The NB source model is the NUBEAM orbit following Monte Carlo [30, 31]. The NB source has 1 MeV particle energy, with the capability to steer from on-axis to off-axis. It is found that keeping one beam on-axis does affect the evolution of the current profile particularly in the first 500 s of the discharge, limiting the increase of $q(0)$. Unless otherwise stated, sll simulations shown herein use one beam on-axis and one-beam off-axis. With this steering configuration the deposition profiles peak at normalized radius $\rho \sim 0.3$, and the NB provides about 2.0-2.5 MA of driven current, depending on the scenario.

*Electron Cyclotron model* The electron cyclotron heating and current drive are calculated with the GENRAY toroidal ray tracing code [32, 33], which has been combined with an adjoint calculation of the electron cyclotron current drive efficiency [34, 35], which includes relativistic effects, trapped particle effects and momentum conserving corrections to the background collision operator. The ITER electron cyclotron system will use 20 MW in its baseline configuration for heating and current drive, which can be diverted to either an equatorial launcher (EL) or an upper launcher (UL) by means of a switch in the transmission line [36]. The EL has three lines of injection, of which one will be injecting waves in the counter-current drive direction. Only the co-current lines are used in the simulations presented herein. The UL - designed for Neoclassical Tearing Mode stabilization - has highly localized off-axis deposition at $\rho = 0.45 - 0.8$ distributing the power in two rows: an upper (USM) and a lower (LSM) steering mirror [36, 37]. Compared to the other sources the EC has unique flexibility for deposition control.

*Lower Hybrid Heating and Current drive* Among the RF sources, the LH has the highest current drive efficiency and it deposits far off-axis, where it is beneficial for setting the ITB foot at large radii. The simulations described herein use GENRAY to compute the LH wave propagation and an adjoint calculation of the LH current drive efficiency [34, 35]. The LH power spectrum uses a 72.5% forward and 27.5% backward power and a parallel refractive index $n_{\|}$ between 1.75 and 1.85. GENRAY accounts for the poloidal distribution of the LH waveguide array by distributing rays along the full vertical extent of the launcher. The distributed launch employed in GENRAY is crucial

for accurate simulation of the LH wave propagation and absorption since the parallel wavenumber evolution of LH ray trajectories is sensitive to their initial poloidal launch point.

Time-dependent scenario simulations use the SWIM-IPS framework [25, 26] for the RF calculations and TRANSP [27] for the NB calculations. This is because the NUBEAM module includes the radial electrostatic potential in the calculation of the beam deposition. TRANSP uses the NCLASS module for the calculation of the poloidal rotation profiles, which is not implemented in the IPS. Therefore, the time-dependent scenario calculated in the IPS is given to TRANSP for calculation of the NB heating and current drive profiles and of the total MHD pressure and rotation profiles (which are used for the calculation of the thermal diffusivity); these profiles from TRANSP are given back to TSC for re-calculation of the scenario within the IPS framework.

### *2.2. Transport models*

To simulate the ITB formation and dynamics we use the CDBM (Current Diffusive Ballooning Mode) model [38]. This model is based on the theory of self-sustained turbulence due to current diffusivity driven modes [39]. The thermal diffusivities are computed as the sum of a neoclassical and a turbulence term $\chi_{\rm T}$ [38, 40]:

$$\chi_{\rm T} = 12\ F(s,\hat{\alpha}) F_\kappa F_{\rm E} \alpha^{3/2} \frac{c^2}{\omega_{\rm pe}^2} \frac{v_{\rm A}}{qR} \tag{1}$$

where $c$ is the speed of light, $\omega_{\rm pe}$ the electron plasma frequency, $v_{\rm A}$ the Alfvén velocity and $\alpha \equiv -q^2 R(d\beta/dr)$ the normalized pressure gradient. The same $\chi_{\rm T}$ holds both for ions and electrons, since the CDBM model does not distinguish between species. The constant in $\chi_{\rm T}$ provides the correction between the CDBM confinement time and the ITER $\tau_{89}$ confinement scaling [38]. The factor $F(s,\hat{\alpha})$ represents the reduction in the thermal diffusivity due to weak or negative magnetic shear and large Shafranov shift [38] and it accounts for about 90% of the transport reduction in these scenarios [41]. It is a function of the magnetic shear $s \equiv rq^{-1}(dq/dr)$ and of the normalized MHD pressure gradient $\hat{\alpha}$, which includes the fast ion contribution [42]. Plasma shape effects are included in the factor $F_\kappa$ [43]. The term $F_{\rm E} = [1 + \omega_{\rm E}^2/\gamma^2]^{-1}$ models the $\mathbf{E}\times\mathbf{B}$ flow shear turbulence stabilization, where $\gamma$ is the growth rate of the most unstable mode [39], $\gamma^{-1} = (6s/\alpha)^{1/2}(qR/v_A)$. The shearing frequency $\omega_{\rm E}$ is defined according to Hahm and Burrell [44], assuming isotropic turbulence in the plane perpendicular to the magnetic field and the radial electric field is derived from the radial ion force balance equation.

We have not benchmarked the CDBM model on present experiments with ITBs (for a recent comparative transport analysis of JET and JT-60U see the work by Garcia *et al* [45]). However, predictive simulations performed on a number of case scenarios with different H/CD mixes and with a range of magnetic shear profiles indicate that the CDBM qualitative reproduces features observed in experiments, such as (1) the flattening of the central temperature in strong reverse shear plasmas, (2) the steepening

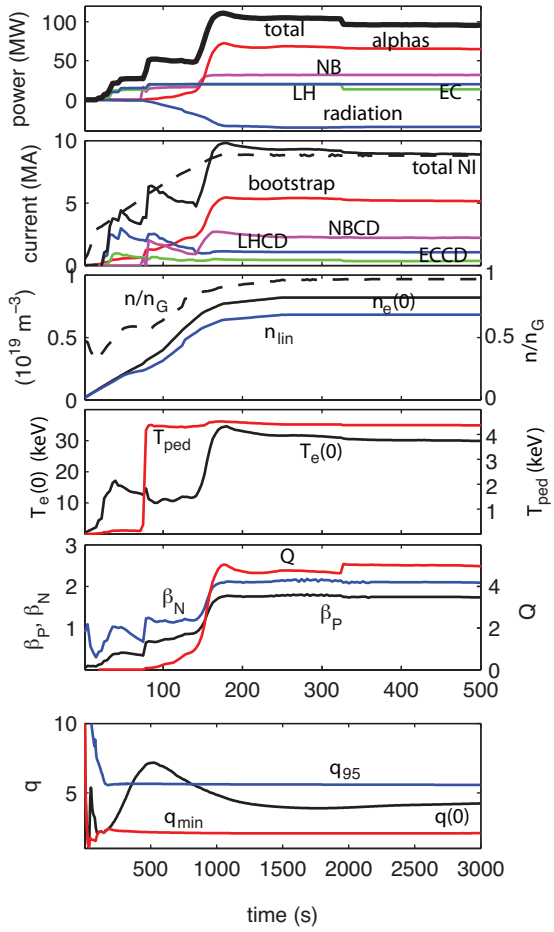


**Figure 1.** Scenario simulation with 33 MW of NB and 20 MW each of EC and LH. (a) External power, alpha power, total power and total radiation; (b) plasma current (dash), non-inductive (black) and bootstrap (red) current, NBCD (magenta), LHCD (blue) and ECCD (green); (c) central and line integrated density and $n_e/n_G$; (d) electron temperature; (e) poloidal $\beta$, normalized $\beta$ and fusion gain $Q$; (f) safety factor on-axis (black) $q_{min}$ (red) and $q_{95}(blue)$. The horizontal axis has been extended to the end of the flattop phase to show the evolution of the safety factor.

of the temperature gradient at the location where the shear is zero [41]; (3) barrier collapse when the shear becomes positive and when $\rho(q_{\rm min}) < 0.25$. For these reasons, we believe that the CDBM is adequate to model the formation and sustainment of ITBs in the steady state scenarios explored herein.

Particle transport models are not used in this work, instead the electron density profiles are prescribed, as the superposition of a broad profile for the H-mode and a peaked profile that models the ITB. The Helium concentration is determined by an input $\tau^*_{\rm He}/\tau_{\rm E} = 5$ and includes the buildup to burn conditions. The Hydrogen (DT) fuel density is determined from quasi-neutrality assuming equal amounts of D and T. The impurity density profiles are assumed to be the same as the electron density, with their fractions prescribed as a function of time. Dominant impurities are Beryllium (2%

fraction of the electron density) and Argon (0.4% fraction), which provide about 40 MW of core radiated power (bremsstrahlung, cyclotron and line radiation).

## 3. Towards stationary solutions with ITB

The ITER steady state scenario depends critically on the heating and current drive sources, since the current profiles, in combination with the bootstrap current, determine the safety factor profile. Steady state operation will need real time control of the current profile in order to sustain weakly reversed or flat magnetic shear in the core, which will sustain wide ITBs at mid-radius.

The formation and sustainment of stationary current and ITBs with the baseline heating mix has been discussed in a previous work [41]. However, since the EC steering configuration used in the simulations presented herein is based on those findings, a short summary of the main results is given in this section.

The far off-axis deposition of the UL makes of this launcher a potential knob for current profile control and for stabilization of the ITB foot in steady state scenarios. Time-dependent simulations were run to explore how the distribution of power between the equatorial and the upper launcher affects the formation and sustainment of magnetic shear profiles reversed in the core and hence the sustainment of ITBs. It was found that delivering power to the EL in the ramp-up phase favors the formation of reverse shear profiles, which trigger the formation of strong electron ITBs. The equatorial launcher has also higher current drive efficiency thus contributing to a higher non-inductive current in the ramp-up phase. Switching from one of the equatorial lines of injection to the upper launcher at the end of the ramp-up phase favors the stabilization of the ITB foot in the flattop. The lower current drive efficiency of the upper launcher is compensated by a larger bootstrap current. It was found that the steering configuration that maximizes the total current (bootstrap plus EC driven current) has two third of the injected power delivered to the upper launcher and the EL deposition close to mid-radius.

By distributing the power between the equatorial and the upper launcher, and with mid-radius deposition of the EL, the baseline heating mix is predicted to sustain stationary ITBs for 3000 s and stationary non-inductive current of up to 6.4 MA, with 100 kA overdrive to sustain moderate reverse shear profiles. With the Coppi-Tang model, modified for ITBs prescription [17] and with fixed $H_{98} = 1.6$, the predicted current increases up to about 7 MA. With $\beta_N$ and fusion gain $Q$ below two, the performance of this plasma is well below the ITER goals. Regardless, the plasma equilibria are predicted to be ideal MHD stable around the operational point even with peaked pressure profiles, making the baseline heating mix a good candidate to demonstrate ITB sustainment and steady state operation at low current [22, 41].

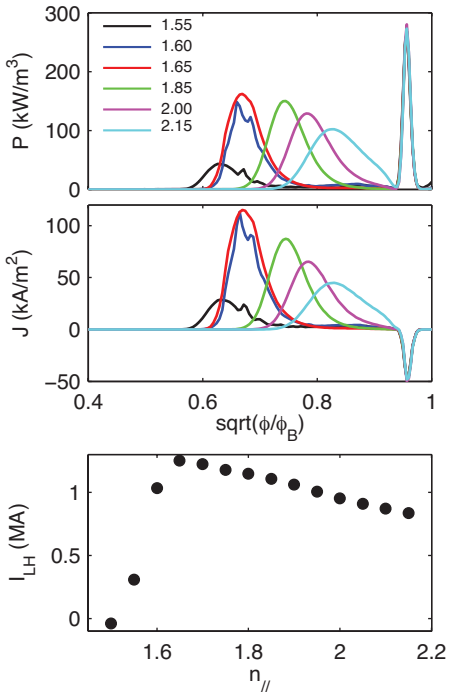


**Figure 2.** (a) power density and (b) parallel current density profiles as a function of the LH spectrum $n_{\|}$. For graphic purpose only a limited number of profile are shown. (c) LH driven current as a function of $n_{\|}$ between 1.50 and 2.15.

## 4. Using LHCD to sustain more expanded ITBs

Off-axis lower hybrid current drive has been successfully used to develop candidates for steady state scenarios on JET, JT-60U and Tore Supra [46]. The sustainment of stationary ITBs for times close to the current resistive time (11 s, *i.e.* $\simeq 37\tau_E$) has been demonstrated on JET with off-axis LHCD and with NBCD and ICRH, sustaining about 80% of non-inductive current and $\beta_N \simeq 1.7$ [9].

This section discusses the use of LH heating and current drive in the ITER steady state scenarios to sustain higher non-inductive current and more expanded ITBs. It will be shown that the LH is effective at setting the ITB foot at large normalized radius, thus triggering and sustaining expanded ITBs, and that the EC - providing additional current inside the LH deposition region - freezes the bootstrap current profiles, which peak at mid-radius stabilizing the ITB foot.

### *4.1. Selection of the LH refraction index*

Figure 2 shows the deposition profile and LH driven current for values of $n_{\|}$ between 1.50 and 2.15. These simulations have been run in the flattop starting from the same equilibrium and kinetic profiles, from a configuration with 20 MW of EC and 20 MW of LH with $n_{\|} = 2.15$ [47] and the discharge has been evolved between 1000-1500 s to relax the current profiles. The calculations self-consistently evolve the LH and the EC

profiles, but use the same NB heating and deposition profiles (from TRANSP). It should be expected that, for a complete discharge evolution simulation where the correct NB profiles are included in the loop, results may change from what is shown in the figure, particularly at lower $n_\parallel$ values. For the range of central densities explored in this work, $n_e \simeq (7.0 - 8.2) \times 10^{19}$ m$^{-3}$, the LH accessibility condition gives $n_\parallel > 1.63 - 1.67$.

The deposition profiles shown in Fig.2 show evidence of incomplete single pass absorption when $n_\parallel < 1.65$. Here the slow wave either converts to a fast wave and propagates to the edge or remains a slow wave and still propagates to the edge. This causes an edge reflection that is accompanied by a large $n_\parallel$ upshift and absorption far off-axis.

A maximum in the driven current is observed for $n_\parallel = 1.65$, with $I_{LH} = 1.25$ MA compared to 1.0 MA for $n_\parallel = 1.9$ and 0.85 MA for $n_\parallel = 2.15$. The difference in LHCD between the case with $n_\parallel = 1.65$ and the case with $n_\parallel = 1.95$, which is the largest parallel wavenumber value at which the LH driven current remains above 1 MA, is 250 kA, namely about 20% of the total LH driven current and about 4% of the total non-inductive current. However, at the low temperatures typical of the early ramp-up phase, low values of the parallel wavenumber will affect the LH wave penetration. The electron Landau damping condition $T_e = 40/n_\parallel$ gives 14.7 keV for $n_\parallel = 1.65$ and 11.7 keV for $n_\parallel = 1.85$. This makes a small difference in the L-mode evolution, with the exception of the very early L-mode evolution, with LH waves being absorbed for all parallel refractive index values starting from about 5-10 s of RF heating after divert time.

### *4.2. Configuration with 20MW each of EC and LH in the flattop*

We have run a simulation scenario that uses in the flattop 20MW of EC combined with 20MW of LH and 33MW of NB. This heating mix configuration has been previously described in Refs. [16, 22]. The main differences with previous works are: (1) the confinement gain is not constrained to satisfy $H_{98} = 1.6$, (2) these simulations use the CDBM model instead of Coppi-Tang, thus the thermal diffusivity profile is evolved dynamically (3) the EC power is distributed among the equatorial and the upper launcher instead of being all delivered to the equatorial launcher and (4) the LH heating and current drive is calculated using GENRAY instead of LSC. The capability of having GENRAY implemented for both the LH and the EC calculations in a time-dependent simulation was not available at that time and it represents a significant improvement in the present prediction capabilities.

The LH wave refractive index value affects the deposition radius. As shown in Fig.2, the deposition peak of the forward lobe in the flattop moves from $\rho = 0.68$ when $n_\parallel = 1.65$ to $\rho = 0.75$ when $n_\parallel = 1.85$. Although inner penetration is desirable for higher current drive efficiency, the heating and current density profiles for lower wavenumber are almost aligned with the radius where the CD efficiency of the UL is maximum. Since one aim of this work is to explore the benefits from all external sources, in order to maximize the radial coverage the H/CD sources we will operate the LH with

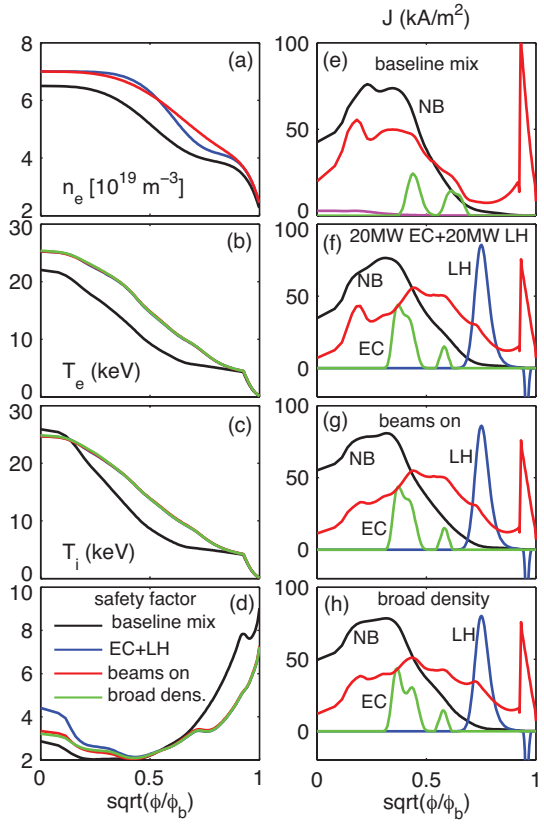


**Figure 3.** left: profiles of density, temperature and safety factor for the baseline scenario (black) and for three configurations with 20MW each of EC and LH. Right: profiles of parallel current density: bootstrap (red), LHCD (blue), ECCD (green), NBCD (black) and FWCD (magenta).

$n_\parallel = 1.85$. The loss of LHCD is about 10% compared to the maximum current with $n_\parallel = 1.65$ as shown in Fig.2 and the loss of total driven current is about 2%. On the other hand, the LH and the EC deposition profiles do not superpose, allowing more flexibility in the radial distribution of the externally driven current.

Figure 3 compares the heating and kinetic profiles of this configuration with the baseline heating mix. The plasma parameters are reported in the first two columns of Table 1. Contrary to the baseline heating mix case, in the flattop phase only one third of the EC power is delivered to the upper launcher. In this case, in fact, the large off-axis current drive from the LH sets the ITB foot at large radii and the upper launcher is used to fill-in the radial region between the equatorial launcher and the LH. The UL (USM) has toroidal and poloidal angle of 20° and 55° respectively. A poloidal steering angle of 100-105 degrees is used for the equatorial launcher (bottom line) and of 80° (top line) to deposit in the range of $\rho = 0.4 - 0.5$. The figure also shows one case with both beams steered on-axis and one case with broader density profile (density peaking factor 1.3 instead of 1.45), which also has both beams steered on-axis. As shown in the figure, no appreciable differences are seen in the temperature and safety factor profiles

**Table 1.** Plasma parameters calculated at $t = 2500$ s. The first column refers to the baseline configuration, the second column replaces IC with LH and keeps the same level of EC and NB heating. The last two columns show configurations where the LH power is progressively increased to 30MW and to 40MW Quantities in bold fonts are input to TSC, like the requested plasma current waveform $I_{\rm P}$.

| | | | | | | |
|---|---|---|---|---|---|---|
| NB (MW) | 33 | 33 | 33 | **33** | 33 | 33 |
| IC (MW) | 20→ 5 | / | / | / | / | / |
| EC (MW) | 20 | 20 | 20 | **13.4** | 13.4 | 13.4 |
| LH (MW) | / | 20 | 20 | **20** | 30 | 30 |
| $n_{\parallel}$ | / | 1.85 | 1.85 | **1.75** | 1.85 | 1.75 |
| **$I_{\rm P}$ (MA)** | 6.3 | 8.5 | 8.6 | 8.8±0.2 | 9.0 | 9.0 |
| $I_{\rm NI}$ (MA) | 6.4 | 8.2 | 8.7 | 8.8±0.2 | 9.2 | 9.2 |
| $I_{\rm BS}$ (MA) | 3.5 | 4.0 | 5.1 | 5.0±0.2 | 5.0 | 5.0 |
| $I_{\rm NB}$ (MA) | 2.45 | 2.5 | 2.1 | 2.2 | 2.1 | 2.1 |
| $I_{\rm EC}$ (MA) | 0.36 | 0.48 | 0.43 | 0.35 | 0.35 | 0.36 |
| $I_{\rm LH}$ (MA) | / | 1.1 | 0.94 | 1.1 | 1.6 | 1.6 |
| $P_\alpha(MW)$ | 23 | 41 | 63 | 65 | 63 | 63 |
| $Q$ | 1.7 | 2.9 | 4.3 | 5.0 | 4.2 | 4.2 |
| $n/n_G$ | 1.0 | 0.86 | 1.0 | 1.00 | 0.96 | 0.96 |
| $T(0)$ (keV) | 23 | 25 | 28 | 29 | 28 | 28 |
| $l_i(1)$ | 0.95 | 0.82 | 0.78 | 0.81±0.01 | 0.77 | 0.78 |
| $q(0)$ | 4.03 | 4.4 | 6.8 | 4.2 (6.1 2.9) | 5.4 | 5.4 |
| $q_{min}$ | 2.02 | 2.1 | 2.2 | 2.09 (2.24 1.99) | 2.2 | 2.2 |
| $q_{95}$ | 8.05 | 5.6 | 5.7 | 5.57 (5.75 5.41) | 5.4 | 5.4 |
| $\beta_{\rm N}$ | 1.77 | 1.78 | 2.2 | 2.3±0.2 | 1.9 | 1.9 |
| $H_{98}$ | 1.38 | 1.42 | 1.62 | 1.65±0.3 | 1.54 | 1.54 |
| $F = H_{89}\beta_N/q_{95}^2$ | 0.1 | 0.15 | 0.20 | 0.21±0.1 | 0.19 | 0.19 |

between the broad and peaked profile cases. Steering both beams on-axis affects mainly the safety factor profile in the inner mid-radius, but it leads to only 1% variation on the global plasma parameters, which are not therefore reported in Table 1.

The reverse current lobe from the LH reduces the height of the pedestal bootstrap current. This affects the safety factor profile at the edge, which does not develop a local minimum aligned with the maximum bootstrap current, as visible instead in the baseline heating mix case (Fig.3d, black curve). A flattening in the $q$ profile is observed at $\rho \simeq 0.75$, where the LH current profiles peak; this reduces the thermal diffusivity off-axis, contrasting the inward diffusion of the ITB foot.

With two-third of power to the equatorial launcher, this configuration scenario with LH has about 25% higher EC driven current compared to the baseline heating mix, *i.e.* 480kA compared to 360kA. Since the LH forms more expanded ITBs, compared to the baseline heating mix configuration the EC equatorial launcher also has higher current

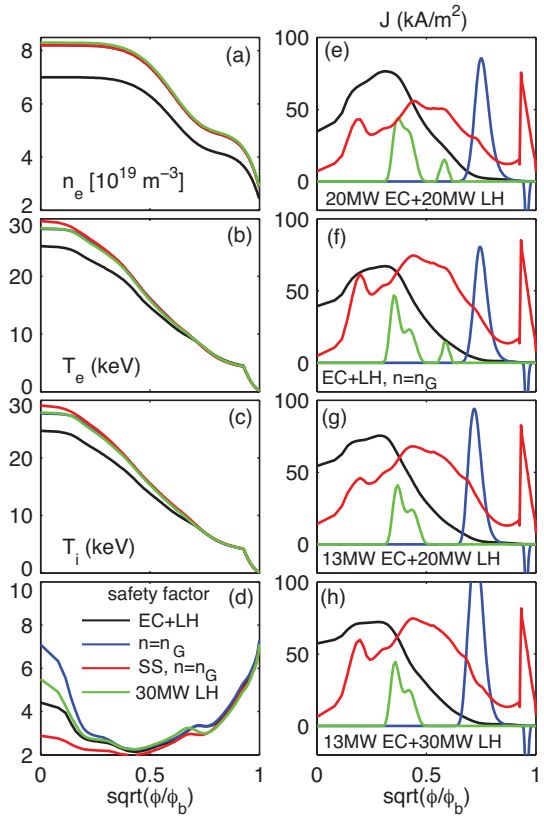


**Figure 4.** Left: profiles of density, temperature and safety factor of configurations with EC and LH heating and current drive. Right: current density profiles.

drive efficiency in the region of $\rho \simeq 0.3 - 0.5$, because temperature profiles are broader and the temperature is higher at this location. This makes the EC more effective at modifying the current and kinetic pressure profiles for variations of the poloidal steering angle. As shown in Fig.3, the bootstrap current profiles are peaked at larger radii in all configurations shown that combine EC and LH, compared to the baseline heating mix.

To summarize, using LHCD sets the ITB foot at large radius and sustains more expanded ITBs. This, in turn, improves the confinement, the alpha heating, sustains non-inductive current above 8 MA and achieves higher confinement and fusion gain. However, the fusion gain, although higher than the baseline heating configuration, is still below 3 and the confinement and $\beta_N$ have marginally improved, as seen from a comparison between column I and II in Table 1.

When the same scenario is modeled with prescribed global confinement multiplier of $H_{98} = 1.6$, either with the CDBM model or with a modified Coppi-Tang model, the total non-inductive current increases to 9MA and the fusion gain to $Q = 3.7$, indicating that confinement improvement is a necessary condition towards the ITER goals.

## 5. Towards the ITER goals

The dimensionless parameter $F = H_{89}\beta_N/q_{95}^2$ is a measure of the performance in a tokamak, which is affected by three key parameters: the confinement, the pressure limit and the limit to increasing plasma current [1].

Compared to the baseline heating mix configuration, wich attains $F = 0.1$, the scenario with LH improves performance by about 50%, achieving $F = 0.15$. However, with 50% bootstrap fraction, $H_{98} \simeq 1.42$ and $\beta_N \simeq 1.78$, this plasma is still below the ITER goals.

Since the fusion power scales with the squared of density, performance can be improved by increasing the electron density close to the Greenwald limit. Higher density will increase the bootstrap current, but on the other hand will decrease the current drive efficiency of the EC and of the NB sources. In order to improve the confinement the ITB foot must be stabilized and the bootstrap current profile optimized to peak at $\rho \geq 0.5$.

Table 1 reports in column III a configuration with 20 MW each of LH and EC, which operates at the Greenwald density. This case is compared with the scenario described in the previous section in Fig.4. Operating at the Greenwald density this plasma sustains an additional 1 MA of self-generated bootstrap current, it has normalized pressure $\beta_N = 2.2$, improved confinement gain $H_{98} \simeq 1.6$ and fusion gain $Q = 4.3$, values that are getting closer to the ITER target. The minimum safety factor is maintained above 2 for the whole discharge, which makes these plasmas ideal MHD stable to the $n = 1$ external kink mode without a wall. It should be noted that the magnetic shear profile is strongly reversed in the core, which might be an issue for energetic particle driven instabilities (not analyzed in this work). The safety factor on-axis can be reduced either by steering both beams on-axis or by setting higher plasma current (as discussed below).

Columns 5-6 in Table 1 reports a case with 30 MW of LH, where the total EC power has been reduced in the flattop to 13.4 MW in order to (1) maintain the total power load to the divertor below 100 MW and (2) maintain almost constant external power to minimize the reduction of the fusion gain, which is calculated as $Q = 5\ P_\alpha/P_{\rm aux}$. Increasing the LH injected (and coupled) power from 20 to 30 MW raises the non-inductive current above 9 MA. However, the bootstrap current, the alpha power and the fusion gain display no improvement with respect to having 20 MW each of LH and EC, suggesting a saturation of the benefits of using LHCD. With about 200 kA current overdrive these configurations with 30 MW of LH have large $q(0)$ because of the counter-current contribution form the ohmic drive.

The last case shown in Table 1 (column IV) and in Fig. 4 is also using 20 MW of EC and of LH, but the LH wave refractive index has been reduced from 1.85 to 1.75. This favors better radial penetration of the LH wave and higher driven current, which increases from 0.94 to 1.1 MA. At this location the LH deposits at $\rho \simeq 0.7$ (see Fig.4), which is very close to the UL deposition radius. The UL has been switched-off in the flattop; this launcher is delivering only 6.7 MW and is the external source with the lowest current drive efficiency. This automatically increases $Q$ through the reduction of

the external power, as also shown in the step-up of $Q$ at 250 s, when the EC power is stepped down from 20 to 13.4 MW. This configuration has higher temperature, which contributes to an increase in the alpha power and thus to higher fusion gain values.
For this configuration we have run the IPS-TRANSP loop for three cases, one with 100% non-inductive current of 8.8 MA and two cases with plasma current of 8.6 MA and 9.0 MA. The range of variation of the solutions for these cases is shown in the Table as an error when the variations are symmetric with the respect to the fully non-inductive solution. For the safety factor the variation is not symmetric and both solutions are reported.

The largest discrepancies in the non-inductive current calculated in the scenario simulations originate from the mismatch between the target plasma current (input to TSC) and the non-inductive current, which dynamically affect the discharge evolution. The ohmic system will provide the current difference between the non-inductive current and the requested waveform, which will be in the co- or counter-current direction depending on the non-inductive current being lower or higher than the target plasma current. The ohmic current contribution changes the safety factor in the core, which directly affect the CDBM model response through the reverse shear parametric dependence $f(s, \hat{\alpha})$. A co-current from the ohmic drive decreases the safety factor on-axis weakening ITBs (and leading to the ITB collapse in case of strong underdrive), while counter-current from the ohmic drive increases $q(0)$ and strengthens the ITBs. Although stronger ITBs have a benefit of a higher global confinement gain, high values of $q(0)$ may lead to energetic particle induced instabilities and to ideal MHD instabilities. A mild overdrive can be beneficial to sustain magnetic shear profiles reversed in the core that help sustaining internal barriers and recharging the ohmic system.

These simulations indicate that the baseline 20 MW of EC with an upgrade of 20 MW of coupled LH is a viable route towards steady state operation in ITER. Operating at densities close to the Greenwald limit and with LH wave refractive index in the range of 1.75-1.85, the plasma can sustain 8.6-9.0 MA of non-inductive current, global confinement with $H_{98} \simeq 1.6 - 1.67$, normalized pressure $\beta_N \simeq 2.1 - 2.5$ and fusion gain of $Q \simeq 4.3 - 5$, with a figure of merit of $F = 0.20$, all values close to the ITER target.

## 6. Upgrades to the baseline heating mix

Upgrades of the ITER heating and current drive sources foresee up to 40MW of LH in a later phase [48]. The simulations discussed in this section aim at answering the question whether 40 MW of LH is better than 20 MW each of EC and LH towards the ITER steady state operation.

### *6.1. Configurations with 40 MW of LH*

Table 2 reports the plasma parameters for four simulations that use 33 MW of NB, 40MW of LH and 20MW of IC, the latter dropped to 5MW in the flattop to maintain

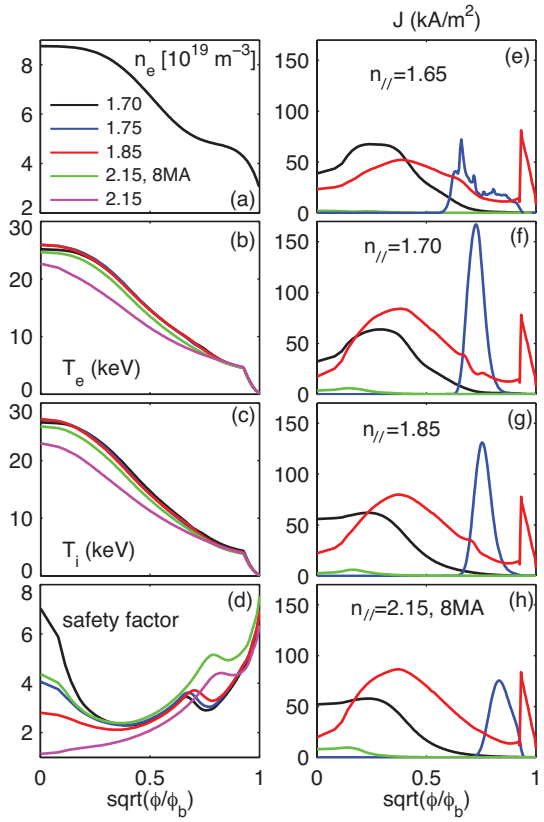


**Figure 5.** Left: profiles of density, temperature and safety factor of configurations with IC and LH heating and current drive. Density profiles are the same in all cases. Right: current density profiles. The case with $n_{\|} = 1.65$ (top) is not reported on the left column.

seed current in the core. The total power in the flattop in these configurations is therefore 5 MW higher than in the case of the reference configuration with EC+LH (reported in column I of Table 1). The corresponding profiles are shown in Fig.5.

These simulations use a parallel refractive index of 1.70, 1.75, 1.85 and 2.15. The total plasma current is 9.0 MA in all cases except the case with $n_{\|} = 1.70$, which has been increased to 9.2 MA to avoid too large a value of $q(0)$ and the case of $n_{\|} = 2.15$, which has been decreased to 8.0 MA to sustain reverse shear in the flattop phase. The results for 9.0 MA for this case are reported in Table 2 for comparison in parentheses and plotted in Fig.5 (magenta curve): the reverse shear (and the internal barrier) is lost within the first third of the flattop phase duration and the confinement decreases close to the typical H-mode confinement levels. A simulation has been run also for $n_{\|} = 1.65$. This case displays evidence for fast wave conversion and is not reported in the table, nor the plasma profiles are shown in Fig.5. However, the LH deposition profile is reported for completeness.

The three configurations with $n_{\|}$ in the range of 1.75-1.85 sustain about 9 MA, with higher LHCD (and non-inductive current) with decreasing the LH wave refractive index.

**Table 2.** Plasma parameters calculated at $t = 2500\,\mathrm{s}$ for configurations with LHCD. Quantities in parentheses refer to results from the Coppi-Tang model. Quantities in bold fonts are input to TSC, like the central density $n(0)$ and the requested plasma current waveform $I_\mathrm{P}$.

| IC (MW) | 20→5 | 20→5 | 20→5 | 20→5 |
|---|---|---|---|---|
| LH (MW) | 40 | 40 | 40 | 40 |
| NB (MW) | 33 | 33 | 33 | 33 |
| $n_\parallel$ | 1.70 | 1.75 | 1.85 | 2.15 |
| **$\mathbf{I_P}$ (MA)** | 9.2 | 9.0 | 9.0 | 8.0 (9.0) |
| $I_\mathrm{NI}$ (MA) | 9.5 | 9.3 | 8.7 | 8.3 (6.6) |
| $I_\mathrm{BS}$ (MA) | 5.0 | 5.2 | 4.9 | 5.2 (3.7) |
| $I_\mathrm{LH}$ (MA) | 2.3 | 2.2 | 2.0 | 1.5 (1.5) |
| $I_\mathrm{NB}$ (MA) | 2.0 | 1.7 | 1.7 | 1.5 (1.3) |
| $I_\mathrm{FW}$ (MA) | 0.05 | 0.06 | 0.05 | 0.07 (0.02) |
| $P_\alpha$ | 59 | 59 | 57 | 54 (43) |
| $Q$ | 3.9 | 3.8 | 3.7 | 3.4 (2.8) |
| $n/n_G$ | 0.91 | 0.93 | 0.93 | 1.05 (0.94) |
| $T(0)$ (keV) | 25 | 26 | 26 | 24 (22) |
| $l_i(1)$ | 0.76 | 0.76 | 0.75 | 0.67 (0.77) |
| $q(0)$ | 6.8 | 3.9 | 2.8 | 4.2 (1.14) |
| $q_{min}$ | 2.30 | 2.31 | 2.11 | 2.36 (1.14) |
| $q_{95}$ | 5.16 | 5.29 | 5.21 | 5.87 (4.90) |
| $\beta_\mathrm{N}$ | 1.68 | 1.80 | 1.75 | 2.37 (1.45) |
| $H_{98}$ | 1.41 | 1.45 | 1.43 | 1.50 (1.23) |
| $F = H_{89}\beta_N/q_{95}^2$ | 0.165 | 0.17 | 0.17 | 0.19 (0.14) |

However, despite of the higher LH current drive efficiency, these configurations with 40 MW of LH do not achieve the same performance as do configurations with 20 MW of EC and 20 MW of coupled LH. The global confinement multiplier is $H_{98} = (1.43 \pm 0.02)$ and $\beta_N = (1.75 \pm 0.06)$, both lower than levels obtained in the configurations with EC operating at similar densities. The fusion gain is also below 4 in these configurations with 40 MW of LH, compared to the steady state case with $Q \sim 5$ in Table 1.

### *6.2. Configurations with upgraded EC power*

The previous sections stressed the advantages of using LH towards steady state operation. One could ask themselves whether an upgrade of EC power would produce plasmas with comparable features of expanded ITBs and high performance as the steady state configuration discussed above.

Comparing the cases shown in columns I-III of Table 1, it can be estimated that,

with 80 kA of current driven by 6.7 MW of EC power to the UL and 940 kA from 20 MW of LH, approximately 70 MW of EC power should be delivered to the UL to drive a comparable current. This, plus 26.8 MW of EC on the EL for mid-radius deposition and current drive and 33 MW of NB would make an unsustainable total of 126 MW of external power, to which the seed current from 5 MW of IC in the flattop should be added. With about 20 MW of core radiated power and 27 MW of alpha power, this configuration would have 150 MW of power load to the divertor. Even with almost 100 MW of injected EC, the total non-inductive current of this configuration is only 7.4 MA, with 3.8 MA from the bootstrap and 1.8 MA from NBCD. The global confinement level is $H_{98} \simeq 1.2$ and the fusion gain is $Q \simeq 1$, much lower than the other configurations analyzed.

Figure 6 compares the profiles of temperature, $q$, the thermal diffusivity, the bootstrap current and the current driven by the EC and by the LH for three cases with different heating mix: a mix of 20 MW each of EC and LH, a mix of IC and 40 MW of LH and the case with 80 MW of EC power to the UL. The steering angle of the UL has been chosen so that the deposition profiles peak at approximately the same location of the LH. Although the current driven far off-axis by 70 MW of EC to the UL and by 20 MW of coupled LH is comparable and about 1 MA, the effect of the two mixing configurations on the thermal diffusivity profile predicted by the CDBM model is much different. Regardless of all three configurations having current peaked at approximately the same radius, the transport is reduced locally in the configuration with an EC upgrade, while it is reduced over a larger region in the two configurations with LH.

The configuration with upgraded EC power uses the same steering angle as the baseline heating mix scenario in the L-mode, with two third of the power on the equatorial launcher and one third on the upper launcher. After the L-H transition, the power is progressively increased to the upper launcher in the ramp-up phase up to 80 MW at the start of the flat-top phase. This configuration sustains stationary current until the end of the flattop phase and the large current to the upper launcher prevents the ITB foot from diffusing inwards, thus confirming the stabilizing role of the EC upper launcher in the sustainment of ITBs. The most important difference between the configurations that use LH from early ramp-up phase and those that do not use LH is in the evolution of the temperature profiles and of the safety factor profiles.

As shown in Fig.7, in configurations with LH, the deposition profiles peak at $\rho \leq 0.3$ in the early ramp-up phase, favoring the formation of reverse magnetic shear profiles and the triggering of ITBs. With increasing density and temperature, the deposition progressively moves outwards and ITBs are progressively expanded. Therefore, all configurations with LH have expanded ITBs and broad temperature profiles at the beginning of the flattop phase. Although the simulations with EC attempt at a progressive steering of the poloidal angle of the EL to deposits at increasingly higher radii while the discharge progresses from ramp-up to flattop, the optimization of the deposition profile in response to the position of the minimum safety factor and of the

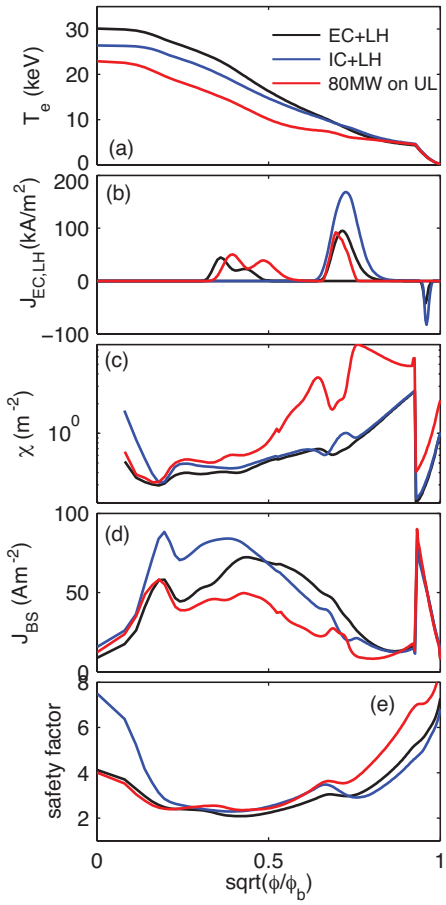


**Figure 6.** Comparison between the configuration with 20 MW each of EC and LH, the configuration with IC and 40 MW of LH and the configuration with 100 MW of EC. (a) Temperature profiles, (b) profiles of LHCD and ECCD, (c) thermal diffusivity, (d) bootstrap current and (e) safety factor.

maximum temperature gradient cannot be optimized at this time because of the absence of a controller in TSC. These results are not therefore a conclusive demonstration that progressive expansion of the ITB is not possible with an upgrade of the EC power. Regardless, because of the lower current drive efficiency of the EC source compared to the LH, it might be difficult to reproduce the same discharge evolution that naturally occurs when using LH with an upgrade of 40 MW of EC, as foreseen for ITER [48].

It is interesting to note that, when the LH is not applied in the early ramp-up phase, but only after the L-H transition, ITBs do have the features of configurations that do not use LH at all, with low non-inductive current and with peaked temperature profiles, indicating that early LH heating and current drive is necessary for both formation and later sustainment of expanded ITBs.

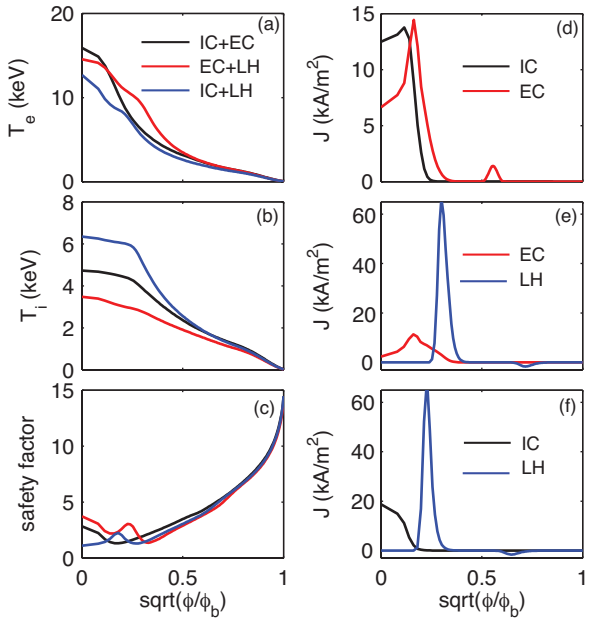


**Figure 7.** Profiles in the ramp-up phase, in L-mode at $t = 50$s for the baseline heating mix configuration, the configuration with 20MW each of EC and LH that reaches steady state and the configuration with 40MW of LH and 5MW of IC in the flattop. Both configurations with LH have $n_{\|} = 1.85$.

## 7. Conclusions

The ITER steady state scenario operation critically depends on the heating and current drive sources, since the current profiles, in combination with the bootstrap current, determine the safety factor profile. In order to achieve the goal of $Q = 5$ with non-inductive current of about 9MA, ITER steady state will need to sustain bootstrap fraction above 50% of the total current and improve the energy confinement times above 50% of the H-mode values. With constrains on the pedestal pressure set by peeling-ballooning instabilities, this will likely be obtainable only in regimes with Internal Transport Barriers.

The heating and current drive sources planned for ITER should be capable of trigger ITBs and sustaining them throughout the flattop, together with stationary, 100% non-inductive current. At the same time, the sources should sustain a weakly reversed shear in the core (to avoid strong ITBs), and have sufficient flexibility to control the position of the minimum safety factor (which sets the ITB foot position in reversed shear magnetic equilibria) and to sustain bootstrap current profiles aligned with the ITB location.

We have studied how the heating and current drive mix affects the bootstrap current profile, the position of the ITB foot, the reduction of transport, towards the realization of steady state operation regimes. Simulations indicate that configurations with a mix of EC and LH (together with 33 MW of NBI) offer an optimum combination of pressure and current density profiles that are compatible with confinement levels

$H_{98} > 1.6$, 55-60% bootstrap fraction and achieve $Q \simeq 5$, thus representing a promising route towards the achievement of the ITER goals. The use of LHCD is necessary for formation and sustainment of expanded ITBs. At the same time the ECCD is important to freeze the bootstrap current profiles and to sustain high global confinement levels. The target steady state configuration has been obtained by optimizing the ramp-up phase for formation of magnetic shear profiles reversed in the core that trigger electron ITBs, but at the same time avoid strong reverse shear profiles that favor ideal MHD instabilities. Particle transport has not been used in these simulations. However, impurity accumulation can be an issue in these discharges with negative magnetic shear and lead to the barrier degradation, as observed on JET [9].

All heating mixes analyzed are capable of forming ITBs and sustaining a stationary non-inductive current in the flattop until the end of the flattop phase. This is obtained with far off-axis current drive, either from the EC upper launcher or from the LH. It is found that the ramp-up evolution is critical for the access to steady state. Simulations indicate in fact that, if LHCD is applied later in the discharge, after the L-H transition, ITBs have features closer to discharges with EC only, with peaked temperature profiles and low non-inductive current and confinement. Injection of LH waves early in the discharge favors a progressive expansion of the barrier and sustainment of higher levels of non-inductive current. It is observed a tendency of the global confinement levels to increase when the heating mix is changed from the baseline mix to a combination of EC and LH and, with the latter, confinement levels increase if the EC deposits at mid-radius.

Scenario simulations are generally affected by several sources of uncertainties. In the absence of a benchmarked particle transport model, density profiles are usually prescribed, in this case as a function of time and a transport model is used to evolve the temperature profile. Although we do not find differences in the relaxed solution within the same transport model when the density peaking factor is changed between 1.35 and 1.5, in order the reduce uncertainties in the ITER scenario predictions these cases should be run with other available transport models, to verify the trends found herein and to define a range of uncertainty in the scenario solution.

It is also important that access to steady state is verified experimentally in today's tokamaks, in regimes of operation relevant to ITER, at densities above 85% of the Greenwald limit, with ITER-like shape and with dominant electron heating and that synergy between the heating and current drive sources is further investigated, as in the studies performed on ASDEX Upgrade [49]. Such experiments are pivotal in the benchmark of models for energy and particle transport, in particular in plasmas with magnetic shear profiles reversed in the core. Finally it is extremely important that the NB and RF actuators continue to be validated against experiment through the use of synthetic diagnostic codes. This provides valuable information on the predictive capability of the simulation models that we use for these actuators (see Section IIA). For example, although the contributions from each actuator to the total current density cannot be separated out, it is possible to compare Motional Stark Effect measurements

of the total current density with what is reconstructed by summing the contributions from each individual actuator model. In addition, the actuator models can be used to simulate experimental diagnostic measurements native to that actuator, such as hard x-ray measurements made during lower hybrid current drive.

## Acknowledgments

This work was supported by the U.S. Department of Energy under contract DE-AC02-CH0911466. ORNL is managed by UT-Battelle, LLC for the U.S. Department of Energy under Contract DE-AC05-00OR22725. Partial support for this work was provided through the Scientific Discovery through Advanced Computing (SciDAC) program, funded by U.S. Department of Energy, Office of Science, Fusion Energy Sciences. This research used resources of the National Energy Research Scientific Computing Center, which is supported by the Office of Science of the U.S. Department of Energy under Contract No. DE-AC02-05CH11231.

[1] C. Gormezano, A. C. C. Sips, T. C. Luce, S. Ide, A. Becoulet, X. Litaudon, A. Isayama, J. Hobirk, M. R. Wade, T. Oikawa, R. Prater, A. Zvonkov, B. Lloyd, T. Suzuki, E. Barbato, P. Bonoli, C. K. Phillips, V. Vdovin, E. Joffrin, T. Casper, J. Ferron, D. MAzon, D. Moreau, R. Budny, C. Kessel, A. Fukuyama, N. Hayashi, F. Imbeaus, M. Murakami, A. R. Polevoi, and H. E. St John. Nucl. Fusion, 47:S285, 2007.

[2] Y. Shimomura, Y. Murakami, A. R. Polevoi, P. Barabaschi, V. Mukhovatov, and M. Shimada. Plasma Phys. Control. Fusion, 43:A385, 2001.

[3] J. W. Connor, T. Fukuda, X. Garbet, C. Gormezano, V. Mukhovatov, M. Wakatani, the ITB Database Group, and the ITPA Topical Group on Transport and Internal Transport Barrier Physics. Nucl. Fusion, 41:1823, 2001.

[4] X. Litaudon. Plasma Phys. Control. Fusion, 48:A1–A34, 2006.

[5] G. M. Staebler. Plasma Phys. Control. Fusion, 40:569, 1998.

[6] R. C. Wolf. Plasma Phys. Control. Fusion, 45:R1–R91, 2003.

[7] M. A. Henderson, Y. Camenen, S. Coda, T. P. Goodman, P. Nikkola, A. Pochelon, O. Sauter, and the TSC team. Phys. Rev. Lett., 93:215001, 2004.

[8] T. P. Goodman, R. Behn, Y. Camenen, S. Coda, E. Fable, M. A. Henderson, and et al. Plasma Phys. Controlled Fusion, 47:B107, 2005.

[9] X. Litaudon, F. Crisanti, B Alper, J. F. Artaud, and et al. Plasma Phys. Control. Fusion, 44:1057, 2002.

[10] C. D. Challis, X. Litaudon, G. Tresset, and et al. Plasma Phys. Control. Fusion, 44:1031, 2002.

[11] G. M. D. Hogeweij, Y. Baranov, G. D. Conway, S. R. Cortes, and et al. Plasma Phys. Controlled Fusion, 44:1155, 2002.

[12] Y. Kamada. Plasma Phys. Control. Fusion, 42:A65, 2000.

[13] N Oyama, , and the JT-60 team. Nucl. Fusion, 49:104007, 2009.

[14] T. Fujita. Plasma Phys. Control. Fusion, 44:A19, 2002.

[15] T. C. Hender, P. Hannequin, B. Alper, T. Hellsten, and et al. Plasma Phys. Control. Fusion, 44:1143, 2002.

[16] C. E. Kessel, A. H. Kritz, T. Rafiq, G. Bateman, D.C. McCune, R.V. Budny, D. Campbell, T. Casper, Y. Gribov, and J. Snipes. Development of the iter advanced steady state and hybrid scenarios. volume ITER/P1-22. Vienna:IAEA, 2010. `http://www-naweb.iaea.org/napc/physics/FEC/FEC2010/papers/itr_p1-22.pdf`.

[17] C. E. Kessel, G. Giruzzi, A. C. C. Sips, R. V. Budny, J. F. Artaud, V. Basiuk, F. Imbeaux,

E. Joffrin, M. Schneider, M. Murakami, T. Luce, H. St John, T. Oikawa, N. Hayashi, T. Takizuka, T. Ozeki, Y.-S. Na, J. M. Park, J. Garcia, and A. A. Tuccillo. Nucl. Fusion, 47:1274, 2007.

[18] J. Garcia, G. Giruzzi, J. F. Artaud, V. Basiuk, J. Decker, F. Imbeaux, Y. Peysson, and M. Schneider. Plasma Phys. Control. Fusion, 50:124032, 2008.

[19] J. Garcia, G. Giruzzi, P. Maget, J.F. Artaud, V. Basiuk, J. Decker, G. Huysmans, F. Imbeaux, Y. Peysson, and M. Schneider. Nucl. Fusion, 50:025025, 2010.

[20] G. Giruzzi, J Garcia, J F Artaud, V Basiuk, J Decker, F Imbeaux, Y Peysson, and M Schneider. Plasma Phys. Control. Fusion, 53:124010, 2011.

[21] M. Murakami, J.M. Park, G. Giruzzi, J. Garcia, P. Bonoli, R.V. Budny, E.J. Doyle, A. Fukuyama, N. Hayashi, M. Honda, A. Hubbard, S. Ide, F. Imbeaux, E.F. Jaeger, T.C. Luce, Y.-S. Na, T. Oikawa, T.H. Osborne, V. Parail, A. Polevoi, R. Prater, A.C.C. Sips, J. Snipes, H.E. St. John, P.B. Snyder, I. Voitsekhovitch, and ITPA/Integrated Operation Scenario Group. Nucl. Fusion, 51:103006, 2011.

[22] F. M. Poli, C. E. Kessel, M. S. Chance, S. J. Jardin, and J. Manickam. Nucl. Fusion, 52:063027, 2012.

[23] S. C. Jardin, J. L. Delucia, and N. Pomphrey. J. Comput. Phys., 66:481, 1986.

[24] P. B. Snyder, N. Aiba, M. Beurskens, R. J. Groebner, L. D. Horton, A. E. Hubbard, J. W. Hughes, G. Huysmans, Y. Kamada, A. Kirk, C. Konz, A. W. Leonard, J. Lonnroth, C. F. Maggi, R. Maingi, T. H. Osborne, N. Oyama, A. Pankin, S. Saarelma, G. Saibene, J. L. Terry, H. Urano, and H. R. Wilson. Nucl. Fusion, 49:085035, 2009.

[25] D. Batchelor, C. Alba, G. Bateman, D. Bernholdt, L. Berry, P. Bonoli, R. Bramley, J. Breslau, M. Chance, J. Chen, M. Choi, W. Elwasif, G. Fu, R. Harvey, E. Jaeger, S. Jardin, T. Jenkins, D. Keyes, S. Klasky, S. Kruger, L. Ku, V. Lynch, D. McCune, J. Ramos, D. Schissel, D. Schnack, and J. Wright. Simulation of wave interactions with mhd. In Journal of Physics: Conference Series, volume 125, page 012039, 2008.

[26] W. R. Elwasiv, D. E. Bernholdt, A. G. Shet, S. S. Foley, R. Bramley, D. B. Batchelor, and L. A. Berry. The design and implementation of the swim integrated plasma simulator. In 18th Euromicro Conference on Parallel, Distributed and Network-based Processing, page 419. IEEE, 2010.

[27] R.J. Hawryluk. An empirical approach to tokamak transport. In B. Coppi *et al*, editor, Physics close to thermonuclear conditions, volume 1, page 19, Brussels, 1980. Commission of the European Communities.

[28] M. Brambilla. A full wave code for ion cyclotron waves in toroidal plasmas. Rep. IPP 5/66 5/66, Max-Planck-Institut fur Plasmaphysik, Garching, 1996.

[29] G. W. Hammett. Fast ion studies of ion cyclotron heating in the PLT tokamak. Doctoral thesis, Princeton University, 1986.

[30] R. J. Goldston, D. C. McCune, H. H. Towner, S. L. Davis, R. J. Hawryluk, and G. L. Schmidt. J. Comput. Phys., 43:61, 1981.

[31] A. Pankin, D. McCune, R. Andre, G. Bateman, and A. Kritz. Comput. Phys. Commun., 159:157, 2004.

[32] R. W. Harvey and M. G. McCoy. In Proceedings of the IAEA Technical Committee on Advances in Simulation and Modeling of Thermonuclear plasmas, page 489, Vienna, 1993. IAEA.

[33] A. P. Smirnov and et al. In Proceedings of the 15th Workshop on ECE and ECRH, page 301. World scientific, 2009.

[34] C. F. F. Karney and N. J. Fisch. Phys. Plasmas, 28:116, 1985.

[35] C. F. F. Karney, N. J. Fisch, and A. H. Reiman. In R. McWilliams, editor, Radio-Frequency power in plasmas, volume 190, page 430, New York, 1989. AIP Conf. Proc.

[36] M. A. Henderson, R. Chavan, R. Bertizzolo, D. Campbell, J. Duron, F. Dolizy, R. Heidinger, J.-D. Landis, G. Saibene, F. Sanchez, A. Serikov, H. Shidara, and P. Spaeh. Fusion Science and Technology, 53:139, 2008.

[37] G. Ramponi, D. Farina, M. A. Henderson, E. Poli, G. Saibene, and H. Zohm. Fusion Science and

Technology, 52:193, 2007.
[38] A. Fukuyama, K. Itoh, S-I Itoh, M. Yagi, and M. Azumi. Plasma Phys. Control. Fusion, 37:611, 1995.
[39] K. Itoh, M. Yagi, S-I Itoh, A. Fukuyama, and M. Azumi. Plasma Phys. Control. Fusion, 35:543, 1993.
[40] A. Fukuyama, S. Takatsuka, S-I Itoh, M. Yagi, and K. Itoh. Plasma Phys. Control. Fusion, 40:653, 1998.
[41] F. M. Poli and C. E. Kessel. Phys. Plasmas, 20:056105, 2013.
[42] *Modification of CDBM trransport model and its impact on JT-60U experimental analysis and ITER predictio*n, presented at the 8th ITPA-IOS meeting, Apr 2012, Madrid.
[43] M. Honda and A. Fukuyama. Nucl. Fusion, 46:580, 2006.
[44] T S Hahm and K. H. Burrell. Phys. Plasmas, 2:1648, 1995.
[45] J. Garcia, N. Hayashi, G. Giruzzi, M. Schneider, E. Joffrin, S. Ide, Y. Sakamoto, T. Suzuki, H. Urano, the JT-60U Team, and JET EFDA contributors. Comparative transport analysis of jet and jt-60u discharges. volume P5.057. Stockholm, 2012.
[46] M. Goniche, L. Amicucci, Y. Baranov, V. Basiuk, G. Calabro, A. Cardinali, and et al. Plasma Phys. Contr. Fusion, 52:124031, 2010.
[47] F. M. Poli, P. T. Bonoli, C. E. Kessel, D. B. Batchelor, M. Gorelenkova, R. Harvey, and Y. Petrov. AIP Conference Proceedings, 2013.
[48] D. Bora. AIP Conference Proceedings, 933:25, 2007.
[49] F. Sommer, J. Stober, C. Angioni, M. Bernert, A. Burckhart, V. Bobkov, R. Fischer, C. Fuchs, R.M. McDermott, W. Suttrop, E. Viezzer, and the ASDEX Upgrade Team. Nucl. Fusion, 52:114018, 2012.

The Princeton Plasma Physics Laboratory is operated
by Princeton University under contract
with the U.S. Department of Energy.

Information Services
Princeton Plasma Physics Laboratory
P.O. Box 451
Princeton, NJ 08543

Phone: 609-243-2245
Fax: 609-243-2751
e-mail: pppl_info@pppl.gov
Internet Address: http://www.pppl.gov